ACS OMEGA

http://pubs.acs.org/journal/acsodf

Article

Sequestration of Anionic and Cationic Dyes through Thermally Activated Slate and Their Kinetics and Thermodynamic Characteristics

Shah Hussain, Usman Ghani, Shahid Ali Khan, Vineet Tirth, Ali Algahtani, Aiyeshah Alhodaib,* Asad Ali, Fozia Sultana, Muhammad Mushtaq, and Abid Zaman*

Cite This: *ACS Omega* 2022, 7, 12212−12221

Read Online

ACCESS | Metrics & More | Article Recommendations

ABSTRACT: Adsorption is one of the most common and most robust techniques for the decontamination approach of effluents, owing to its design flexibility, simplicity, cost effectiveness, and high efficiency. However, its application is limited on a large scale due to its cost. The current study investigates the use of low-cost, ecofriendly, and ubiquitous thermally activated clay material. Thermally treated clay was used for the adsorption of crystal violet (CV), Congo red (CR), and malachite green (MG) organic dyes from aqueous solutions. Characterization of slate was carried out with Fourier transform infrared spectroscopy (FTIR), field emission scanning electron microscopy, X-ray diffraction, N_2 physisorption, and XRF spectrometry. The adsorption process was studied as a function of concentration, time, pH, and temperature. Using the batch adsorption technique, the experimentally obtained adsorption data were fitted to both Langmuir and Freundlich isotherms. The adsorption data followed the pseudo-second-order kinetics, and the adsorption capacity was recorded as 360.12 mg/g for CV, 409.23 mg/g for CR, and 390.14 mg/g for MG. The good uptake is the outcome of a greater surface area (24.751 m^2/g) for the slate activated at 873 K. The thermodynamic studies showed that the adsorption process remained endothermic and spontaneous. Thermally activated slate proved itself to be an efficient adsorbent and can effectively be used for the removal of textile dyes from the contaminated water, and it is evident from the good uptake of the adsorbate by the adsorbent.

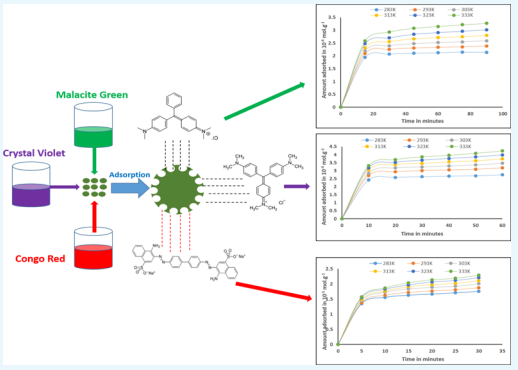

INTRODUCTION

One of the main and serious emerging problems at the global level is the supply of clean water.[1,2] Water resource contamination has increased at an alarming level by various chemical substances due to fast industrialization and uncontrolled practices of irrigation in the field of agriculture.[2,3] Water pollution due to the discharge of untreated or inadequately treated industrial wastewater is a matter of grave concern on the global scale.[4−6] Due to highly visible adverse effects and toxicity, dyes have attracted special attention.[7] The adverse effects of dyes are even prominent at a concentration of 1 ppm sufficient for interfering with the photosynthetic process vital for phytoplankton.[8] The textile industry is one of the worst kinds of polluters for the aquatic system as chemical dyes of different classes besides other chemicals are used in various dyeing processes, a considerable amount of which finds its way into the aquatic system.[6,9−15]

Crystal violet (CV) dye is toxic to such an extent that even 1 ppb of it has a mutagenic effect on humans and animals.[16] CV has also been reported to have teratogenic and mitotic poisoning.[17] Congo red (CR) dye, an azo dye used in the dyeing of silk, wool, paper, and leather, is highly toxic as this dye metabolizes to known human carcinogen benzidine.[18,19] Malachite green (MG) dye is known for serious health hazards; that is why it is banned in Canada and Europe. MG has greater persistency in the environment, and reports have shown that it causes reproductive abnormality in fish and mammals.[20] MG reduces to form leuco-MG which persists in the tissues causing apoptosis and leads to tumor formation.[21] Various materials have been reported in the literature for the adsorption of pollutants from the effluents, including polymer microspheres, polymer hybrid films, inorganic metal oxide, plant-based powder, zeolites, activated carbon, alumina, and various clay minerals.[1,10−12,22,23]

Received: January 29, 2022
Accepted: March 23, 2022
Published: March 31, 2022

Different chemical, physical, and biological techniques including ozonization, coagulation, flocculation, and adsorption have been used for the removal of dyes and other impurities from the contaminated water.[24] Various diverse techniques like electrodialysis and photocatalytic degradation have also been employed for the removal of hazardous dyes from dye-polluted water. Nonetheless, these procedures have been found tedious and non-economical. Owing to higher uptake efficiency and being flexible in operation, adsorption has been found to be the most effective and efficient technique for the treatment of polluted water.[25] Contamination of aquatic systems due to the release of dye-containing effluents from the textile, leather, and paper industries is growing in third world countries like Pakistan, India, and Bangladesh in an unrestrained manner, and no or very little heed is paid to the problem. The objective of this study is upon the assessment and evaluation of cheaply, locally, and abundantly available slate as an adsorbent for the adsorption of industrial dyes CV, CR, and MG.

Population growth increases pollution such as municipal discharge, organic, inorganic, pharmaceuticals, and biological waste to the water resources across the world, which causes illness in both humans and animals. Over the years, researchers have put their efforts to develop and investigate new adsorbents for the effective removal of contaminants from wastewater. Many adsorbents have been reported in the literature for the removal of pollutants; however, still there is a space for introduction and development of new adsorbents for the wastewater treatment. The investigation of new adsorbents is of utmost importance due to the high rate of pollutant discharge in the water beds. Many materials are at the heart of adsorption such as metal oxide, polymer films like chitosan, cellulose, cellulose acetate, and polyethersulfones, polymer nanocomposite films like chitosan−TiO_2, chitosan−zeolite, chitosan−Co_3O_4, and chitosan−ZnO, sand materials like quartzite and clay, plant bag gas like peel of many plants and fruits, and many more. Although these materials displayed a good range of adsorption characteristics against the adsorption of organic and inorganic materials, however, high cost and low resistivity to high temperature restricted their use on a large scale. The only material which shows low cost and high temperature resistivity is the slate materials. Many quartz materials were used for the adsorption of organic and inorganic materials, however, the slate compositions are variable in different regions. Therefore, to the best of our knowledge, the slate materials of Kaka Sahib (a region of District Nowshera, KP, Pakistan) were used for the first time in this study for the adsorption of various anionic and cationic dyes. Therefore, we believe that the exploration of slate of the stated region will be helpful for the adsorption studies (Table 1).

Table 1. Adsorption Capacity Relationship with the Literature Study

adsorbent	dyes	adsorbent capacity (mg g^{-1})	references
rice husk cellulose	diamine green B	207.15	26
peanut hull waste	CV	100.6	27
cotton waste activated carbon	methylene blue	369.48	28
chlorella pyrenoidosa	rhodamine B	63.14	29
aspergillus carbonarius	CR	99.01	30
activated slate	CV	360.12	present work
activated slate	CR	409.23	present work
activated slate	MG	390.14	present work

Table 2. N_2 Physisorption Analysis of Thermally Activated Slate at 873 K

parameters	values
surface area (m^2/g)	24.751
pore volume (cm^3/g)	0.006
pore radius (Å)	14.473

RESULTS AND DISCUSSIONS

Characterization. The surface area, pore volume, and pore radius of the slate were determined through N_2 adsorption−desorption at 77 k[31,32] only for the slate activated at 873 k. It exhibits a specific surface area of 24.751 m^2/g with a pore volume and pore radius of 0.006 cm^3/g and 14.473 Å, respectively, as shown in Table 2

The X-ray fluorescence (XRF) data are depicted in Table 3 which indicate the composition of slate. As obvious from Table 2, SiO_2 is present in the highest weight percentage which is 67.56% followed by Al_2O_3 and Fe_2O_3 which are 15.67 and 5.45%, respectively.

The slate Fourier transform infrared spectroscopy (FTIR) spectrum was recorded in the range 400−4000 cm^{-1}. Different functional groups were analyzed before and after the adsorption of dyes. Noticeable peaks have been observed from 500 to 1600 cm^{-1}. The appearance of the band from 700 to 800 cm^{-1} is due to the bending vibration of O−Si−O, confirming the presence of quartz, while the C−C bending vibrations are in the ∼1000 cm^{-1} range. The subtle difference between the peaks before and after the adsorption confirms the adsorption of these dyes on the surface of the slate as manifested in the inset of Figure 1a−c. The S in the inset of Figure 1a−c stands for activated slate before the adsorption of CV, CR, or MG, and ACV, ACR, and AMG stand for after the adsorption of CV, CR, or MG dyes on the slate at 200−800 °C.

Slate X-ray diffraction (XRD) analysis peaks were recorded from 10 to 70° on the 2θ angle scale. The diffraction pattern of slate exhibited crystalline peaks at 2θ = 20−30° while the crystalline peaks of mullite appeared at 2θ = 50−70°. The diffraction patterns of the slate at different temperatures are same as depicted in the Figure 1d. The FTIR spectrum was plotted in the range of 2000−400 cm^{-1} because outside this region the spectrum is flat.

Field emission scanning electron microscopy (FESEM) micrographs are given in Figure 2a−h, indicating the morphological changes before and after the adsorption of CV dye at 473−1073 K. The changes observed have been highlighted by circles inside the micrographs. The voids in the adsorbent can easily be seen in the micrograph before adsorption. The filling of pores after the adsorption clearly confirms the uptake of the dyes into the pores of the adsorbent as shown in the circle in the micrograph. Similar observations have been observed for CR and MG adsorption at 473−1073 K and are presented in the inset of S1a−h and S2a−h, respectively. A high surface area of 24.751 cm^2/g and a pore volume of 0.006 cm^3/g of the slate activated at 873 K are evident of their high adsorption capacity. The food adsorption capacity of slate activated at 873 K compared to 1073 K is high because at lower temperature, the particle size is small with a greater surface area.

https://doi.org/10.1021/acsomega.2c00611
ACS Omega 2022, 7, 12212−12221

Table 3. Slate Composition Analysis

composition	SiO_2	Al_2O_3	Fe_2O_3	CaO	MgO	K_2O	Na_2O	SO_3
wt (%)	67.56	15.67	5.45	2.71	1.08	2.70	0.13	0.01

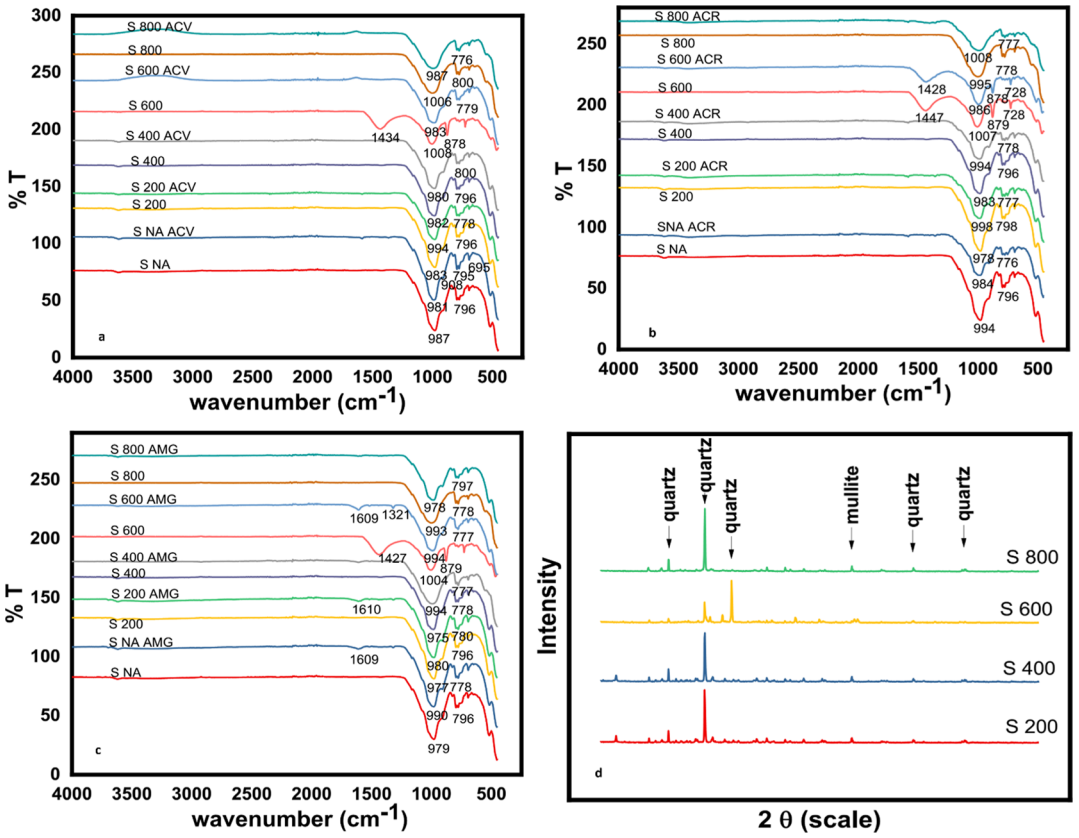

Figure 1. FTIR spectra of slate: (a) before and after adsorption of CV dye, (b) before and after adsorption of CR dye, (c) before and after the adsorption of MG dye, and (d) XRD patterns of slate activated at different temperatures.

Although the slate was also activated below 873 K, if this might be the ideal temperature, which increases the surface area and decreases the particle size, which in turn increases its adsorption capability.

Adsorption Studies and Kinetic Modeling. *Effect of Dye Concentration.* The effect of concentration on the uptake by the adsorbent can be seen from Figure 3a. The amount of the dye adsorbed increased with an increase in the initial dye concentration. With the increase in the concentration of the dye solution, the adsorption increased from 201 to 360 mg/g for CV, 237−409 mg/g for CR, and 220−390 mg/g for MG. The error analysis in all the adsorption experiments was ±1. This increased uptake in the adsorption of all dyes on the surface of slate is due to the concentration gradient and availability of the active sites and pores on the adsorbent surface, which results in greater adsorption.

Effect of Contact Time. The equilibrium contact time for CV adsorption on the adsorbent surface is 0−30 min as shown in Figure 3b and 0−60 min for CR dye Figure 3c while 0−90 min for the MG dye as manifested in Figure 3d. Different equilibration time in the experiments is due to the diverse nature of the dye molecules and different adsorption capacity toward the adsorbent. The brisk adsorption of the dyes in the initial 0−10 min on the surface of the adsorbent is largely due to the greater availability of active sites and pores on the "clean" surface of the adsorbent. The excellent uptake gradually tapers off as the equilibration sits in due to saturation of surface pores and active sites.

Effect of Temperature. With an increase in temperature, an increase in the uptake for all the three dyes has been observed and shown in Figure 3b−d for CV, CR, and MG dyes, respectively. The adsorption capacity enhancement can be attributed to activation of the active sites on the adsorbent surface followed by faster penetration of the molecules of the dyes into the pores of the adsorbent. The adsorption of all the three dyes on the surface of the activated slate has remained physisorption. For instance, the activation energy value for CV is 1.0908 kJ/mole, for CR, it is 0.9644 kJ/mole, and for MG, it is 2.7953 kJ/mole. Physisorption is due to the weak interactions of the dye molecules with the surface of activated slate as presented in following Scheme 1.

Effect of pH. pH plays a vital role in the adsorption characteristics of a material.[33] The removal of CV, CR, and MG at various pH values is provided in Figure 3e. The results indicated that pH of the dye solution considerably affects the removal efficiency of the adsorbent. The removal capability of the slate sample was found to be very low in acidic medium compared to the basic medium. The maximum removal of CV and MG was observed at pH 8.0 while for CR, the recorded optimum pH was 6.0.

Adsorption Isotherms. The adsorption at equilibrium shows the interaction between the adsorbate and adsorbent.

https://doi.org/10.1021/acsomega.2c00611
ACS Omega 2022, 7, 12212−12221

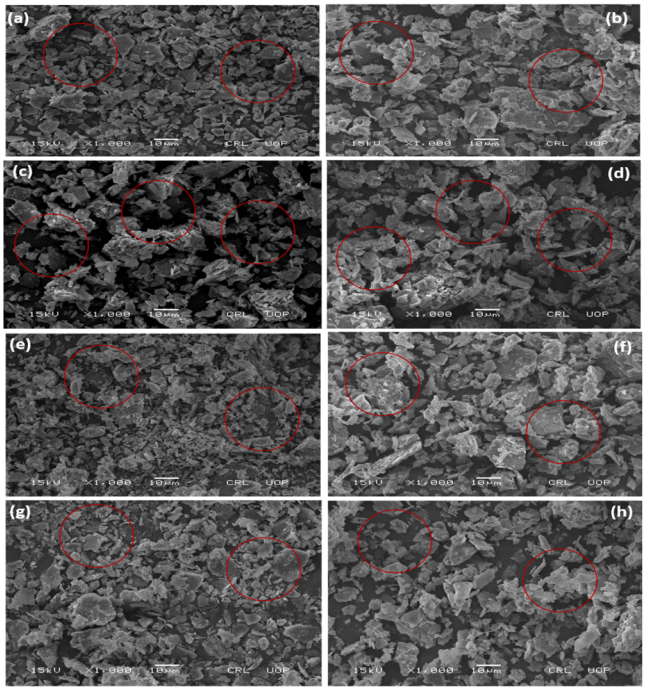

Figure 2. FESEM images of (a,b) slate activated at 200 °C before and after the adsorption of CV, (c,d) slate activated at 400 °C before and after adsorption of CV, (e,f) slate activated at 600 °C before and after the adsorption of CV, and (g,h) slate activated at 800 °C before and after the adsorption of CV dye.

Adsorption process parameters are evaluated using two important isotherm models Freundlich and Langmuir adsorption isotherms. According to the Freundlich model,[10,34,35] the energies and adsorption sites are distributed heterogeneously on the adsorbent surface. The Freundlich equation is given using eq 1.

$$\ln \frac{x}{m} = \ln k + \frac{1}{n} C_e \tag{1}$$

where k (μmol g^{-1}) and $1/n$ (g/dm^3) are the Freundlich constants showing adsorption capacity and adsorption intensity, respectively. The validity of the Freundlich plot is confirmed by the linear plot of ln x/m versus ln C_e. The value of "n" shows the favorability of the adsorption process. According to the Langmuir adsorption isotherm model,[36−38] the various adsorption sites are homogeneously distributed with equal energies. The Langmuir equation is given using eq 2.

$$\frac{C_e}{q_e} = \frac{1}{K_l X_m} + \frac{C_e}{X_m} \tag{2}$$

where C_e represents the equilibrium concentration in mol L^{-1} and q_t represents the amount adsorbed in mol g^{-1} at the time "t". X_m shows the adsorption capacity in mol g^{-1} and is determined from the slope of the plot while the binding constant $0e$ is determined from the intercept of the plot. As stated, the Freundlich adsorption isotherms explain the multilayer and heterogeneous adsorption of the adsorbate on the adsorption surface, while Langmuir adsorption explains the monolayer adsorption of the adsorbate due to the comparable energy of the active sites. Thus, both isotherms are extremely important to explain the surface properties, adsorption mechanism, and affinity of the adsorbent. Freundlich and Langmuir plots for adsorption of CV, CV, and MG on the slate are shown in (a,d), (b,e), and (c,f), respectively. As depicted in these graphs, the R^2 value is higher in the Freundlich adsorption isotherms, thus suggesting the multilayer adsorption of the adsorbate on the surface of slate. The maximum Xm values for CV, CR, and MG as given in Table 4 was found to be 38.75, 169.49, and 55.24 mg·g^{-1}, evident of the accumulation of dye molecules in a greater number to form a saturated layer which might be due to the presence of a greater number of active sites, which enhances the removal ability of CV, CR, and MG by the adsorbent. The value of K_1 provided in Table 4 is showing a gradual increase from 17.27 to 33.96 mg/g for CV, 29.61 to 45.81 mg/g for CR, and 8.616 to 31.78 mg/g for MG with increase in temperature, indicating favorable adsorption.

Kinetics. The adsorption data were analyzed for the kinetic mechanism by applying pseudo-first-order and pseudo-second-order order kinetics as presented in eqs 3 and 4, respectively.

$$\log(q_e - q_t) = -\frac{kt}{2.303} + \log q_e \tag{3}$$

$$\frac{t}{q_t} = \frac{t}{q_e} + \frac{t}{K_2 q_e^2} \tag{4}$$

q_e is the adsorbed amount at equilibrium and q_t shows the adsorbed amount at time "t". In the equation, "k" represents the rate constant which is determined from the $\log(q_e - q_t)$ versus time "t" plot. The pseudo-first-order and second-order kinetics for the adsorption of CV dye is depicted in Figure 5a,b, similarly, for CR dye depicted in (Figure 5d,e) while for MG dye depicted in Figure 5g,h, respectively. Straight lines by the application of the pseudo-first-order equation were obtained as shown in Figure 5, which indicates that the adsorption of these dyes on slate surface obeys the first-order kinetics.

The activation energy for the adsorption process was calculated through the application of the Arrhenius equation[39] as shown in eq 5.

$$\ln k = -\frac{E_a}{RT} \tag{5}$$

K is the rate constant, E_a shows the activation energy, R is the gas constant, and T represents the absolute temperature. The Arrhenius plots for the CV, CR, and MG are given in Figure 4c,f,g, respectively. Values of the "E_a" activation energy calculated by the application of the Arrhenius equation are given in Table 4. The E_a value for CV is 1.090836 kJ/mole, for CR, it is 0.964459 kJ/mole, and for MG, it is 2.795268 kJ/mole.

Thermodynamic Study. The effect of temperature on the adsorption of CV, CR, and MG dyes by the slate adsorbent was studied at different temperatures at 283, 293, 303, 313, 323, and 333 K. The adsorption of the dyes on the adsorbent surface increased, showing the endothermic nature of the adsorption process. The enhancement in the adsorption of the dyes on the surface of the adsorbent is due to the generation of new sites or the faster mobility of the water molecules followed by the accelerated entry of the dye molecules into the slate pores. To further clarify the detailed picture of the adsorption process, various thermodynamic parameters like free energy change (ΔG°), enthalpy change (ΔH°), and entropy change (ΔS°) were calculated from following eqs 6−8, respectively.

$$\Delta G^\circ = \Delta H^\circ - T\Delta S^\circ \tag{6}$$

$$\Delta G^\circ = -RT \ln K_l \tag{7}$$

https://doi.org/10.1021/acsomega.2c00611
ACS Omega 2022, 7, 12212−12221

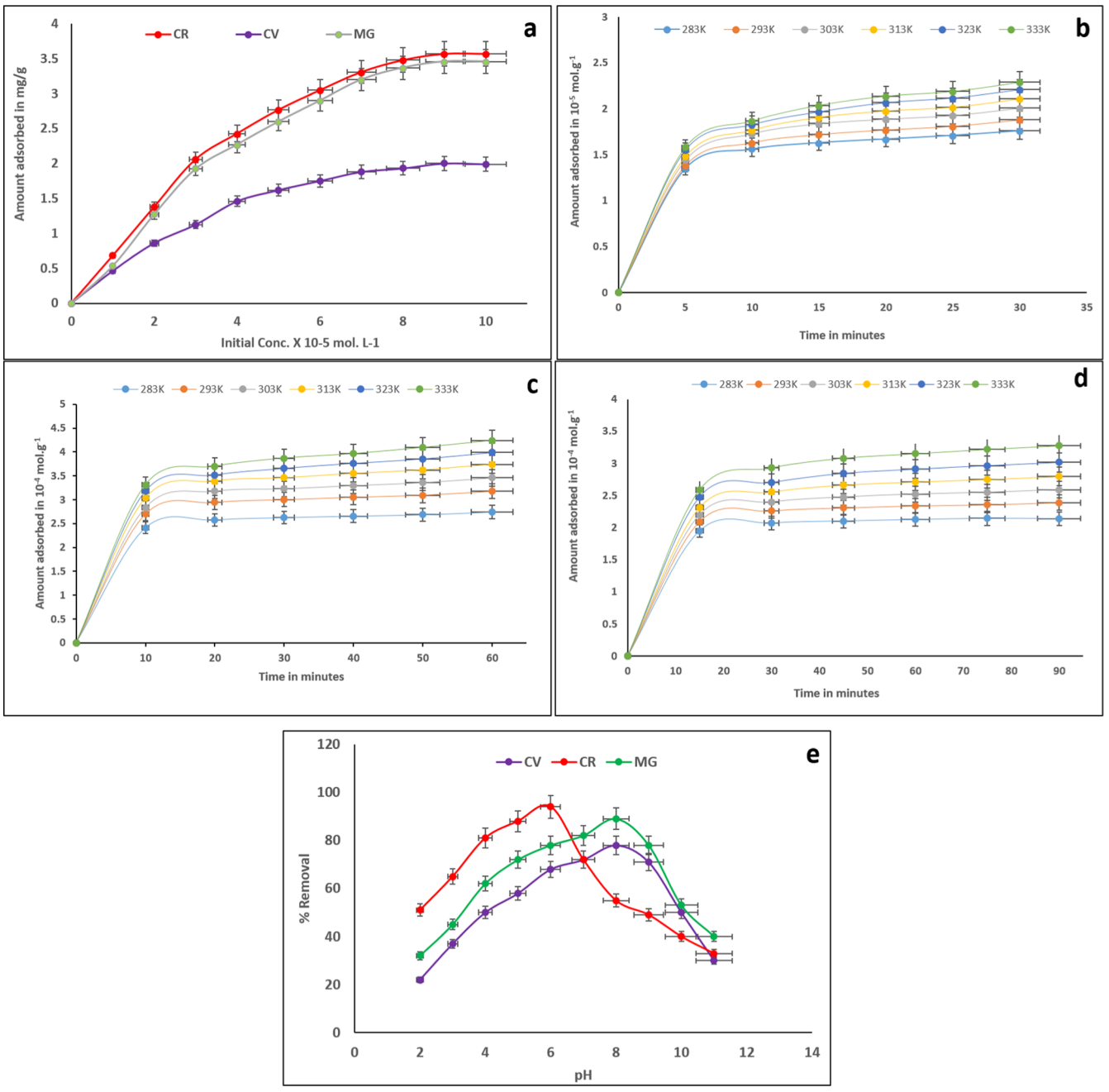

Figure 3. Various optimization steps for dyes adsorption on slate: (a) effect of initial concentration of dyes, (b) effect of contact time and temperature on CV adsorption, (c) effect of contact time and temperature on CR adsorption, (d) effect of contact time and temperature on MG adsorption, and (e) effect of pH on the adsorption of CV, CR, and MG dyes.

Scheme 1. Adsorption of CR Dye on the Surface of Activated Slate through Weak Forces

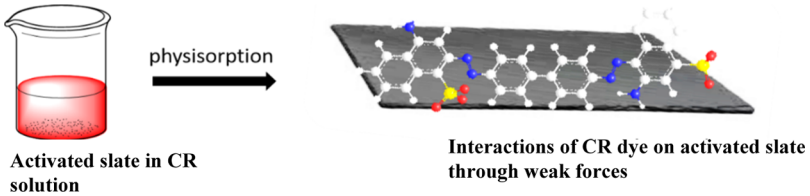

$$\ln K_1 = \frac{\Delta H^\circ}{RT} + \frac{\Delta S^\circ}{R} \quad (8)$$

where K_1 the binding constant is determined from the intercept of Langmuir's equation plot. The favorability and spontaneity of the adsorption process are evident from the negative values of (ΔG°) given in Table 5. The endothermic nature of the adsorption process is evident from the enthalpy change (ΔH°), which has positive values. Structural changes in the adsorbent's

https://doi.org/10.1021/acsomega.2c00611
ACS Omega 2022, 7, 12212−12221

Table 4. Arrhenius Plot for All Dyes Adsorption on Slate

	temp (°C)	Kelvin scale	Kelvin scale $1/T$	Kelvin scale $1/T \times 10^{-3}$	value of k	ln k	E_a (kJ/mole)
CV	10	283	0.0035	3.53	0.0928	−2.3772	1.0908
	20	293	0.0034	3.41	0.0951	−2.3527	
	30	303	0.0033	3.30	0.0956	−2.3479	
	40	313	0.0032	3.19	0.0972	−2.3310	
	50	323	0.0031	3.09	0.0997	−2.3054	
	60	333	0.0030	3.00	0.0990	−2.3123	
CR	10	283	0.0035	3.53	0.0409	−3.1943	0.9645
	20	293	0.0034	3.41	0.0414	−3.1832	
	30	303	0.0033	3.30	0.0419	−3.1721	
	40	313	0.0032	3.19	0.0426	−3.1558	
	50	323	0.0031	3.09	0.0431	−3.1450	
	60	333	0.0030	3.00	0.0435	−3.1344	
MG	10	283	0.0035	3.53	0.0334	−3.3994	2.7953
	20	293	0.0034	3.41	0.0350	−3.3522	
	30	303	0.0033	3.30	0.0368	−3.3009	
	40	313	0.0032	3.19	0.0382	−3.2641	
	50	323	0.0031	3.09	0.0389	−3.2462	
	60	333	0.0030	3.00	0.0398	−3.2228	

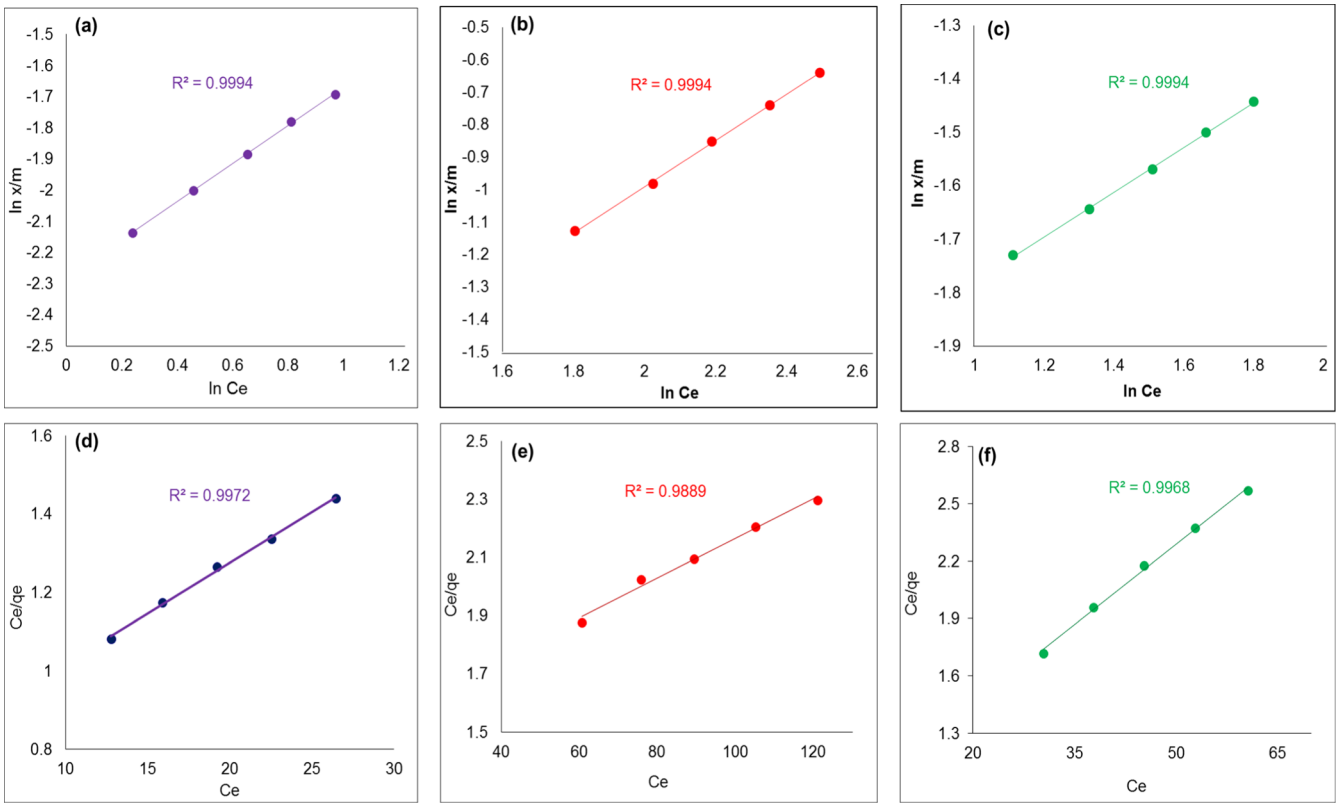

Figure 4. : Freundlich and Langmuir plot for adsorption of (a,d) CV on the slate, (b,e) CR, and (c,f) MG.

active sites are obvious from the FESEM images and have been confirmed by the entropy change (ΔS°) positive values, which show an increase in randomness at the interface of solid and solution. The thermodynamic studies show that the adsorption of CV, CR, and MG dyes on the surface of the slate adsorbent is an endothermic and spontaneous adsorption process.

CONCLUSIONS

This research work reports an ecofriendly, cost-effective, and abundantly available source of clay, which can be effectively utilized for the removal of hazardous chemicals such as textile dyes from the contaminated waters. This study unveils the characteristics of activated slate for the adsorption of CV, CR, and MG dyes. The experimental data fitted best in the pseudo-second-order equation, showing the adsorption rate dependency upon the availability of the adsorption sites. The adsorption experimental data fitted well in Freundlich models. Furthermore, various thermodynamics data revealed that the adsorption process is endothermic and spontaneous in nature. The adsorbent showed good uptake ability toward the dyes, especially CR and MG dyes.

https://doi.org/10.1021/acsomega.2c00611
ACS Omega 2022, 7, 12212−12221

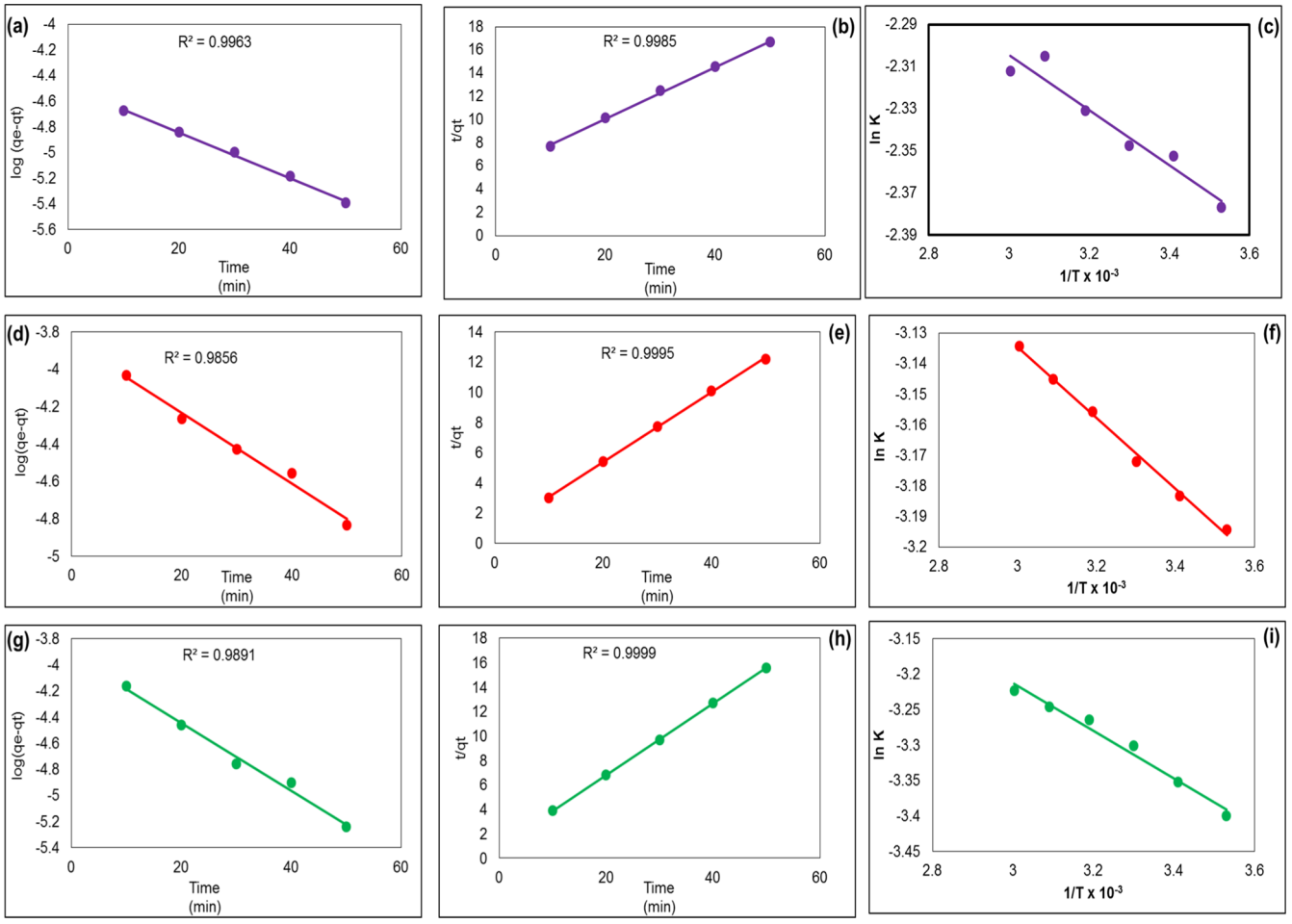

Figure 5. Pseudo-first-order and second-order and Arrhenius plots for adsorption of (a–c) CV dye, (d–f) CR dye, and (g–i) MG dye on the slate.

Table 5. Langmuir Parameters Values for Adsorption of CV, CR, and MG on Slate

	Kelvin $1/T \times 10^{-3}$	X_m (mg·g^{-1})	k_1 (mg·g^{-1})	ln k_1	$\Delta H°$ (kJ/mol)	$\Delta S°$ (J/mol·K)	$\Delta S°$ (kJ/mol·K)	$\Delta G°$ (kJ/mol)
CV	3.53	34.48	17.27	2.8489	11.2077	62.8237	0.0628	−6.5714
	3.41	36.10	18.26	2.9047				−7.1997
	3.30	35.84	22.01	3.0915				−7.8279
	3.19	36.63	25.89	3.2539				−8.4561
	3.09	37.73	29.82	3.3952				−9.0844
	3.00	38.75	33.96	3.5252				−9.7126
CR	3.53	169.49	29.61	3.3881	6.6689	51.8147	0.0518	−7.9947
	3.41	158.73	33.55	3.5130				−8.5128
	3.3	156.25	36.42	3.5951				−9.0319
	3.19	156.25	38.71	3.6561				−9.5491
	3.09	151.51	42.76	3.7556				−10.0673
	3.003	147.05	45.81	3.8245				−10.5854
MG	3.53	55.24	8.616	2.1536	17.8117	81.8260	0.0818	−5.3450
	3.41	40.81	15.009	2.7087				−6.1633
	3.3	39.21	16.803	2.8216				−6.9816
	3.19	41.32	19.064	2.9478				−7.7998
	3.09	39.52	22.971	3.1340				−8.6181
	3.003	35.58	31.78	3.4588				−9.4363

MATERIALS AND METHODS

Materials. CV (analytical grade BDH no. BH151D), CR (analytical grade Sigma-Aldrich no. S241294), and MG (analytical grade Merck no. B581740) were procured and were used without purification. The solutions of all the dyes were prepared in double-distilled deionized water using laboratory water deionizer LABTECH 100 RO Lph. From the stock solutions, working solutions were prepared by dilution. Slate stones were obtained from the kaka sahib rock hills of District Nowshera KPK, Pakistan, situated at the midpoint of the industries to the north and south with gps coordinates of 34° 0′

https://doi.org/10.1021/acsomega.2c00611
ACS Omega 2022, 7, 12212−12221

57.0888″ N and 71° 58′ 31.6164″ E. This area is approximately 15 km away from Nowshera Cantonment.

Sample Preparation. Slate stones obtained were washed with double-distilled water and then dried, crushed, and screened through 250 μm mesh. The collected particles were dried in a vacuum oven for 1 h using the LABTECH LCO-3050H model. The dried and powdered slate was then activated in a temperature range of 200−800 °C in a high-temperature furnace for 30 min to 1 h time interval using a LABTECH LEF-1035-1 furnace. In air-tight Pyrex glass vessels, the samples were stored.

Instrumentation. The N_2 adsorption−desorption isotherms were conducted at liquid-nitrogen temperature (77 K) using model NOVA 2200e. For the composition study, finely powdered clay was analyzed using a Cubix XRF spectrometer (PW2300, Netherland). XRD technique was used to determine the sample crystallinity using an X-ray diffractometer (Rigaku Japan XRD) working at a power of 35 kV and 20 mA with a Cu Kα radiation of 1.5405 nm wavelength. The samples were scanned from the 10 to 80° range of 2θ (degree). Using the model (Shimadzu IR Prestige-21) of the Fourier transform infrared spectrophotometer, the FTIR spectra of the samples were carried out. Sample scanning was carried out in the 4000−400 cm^{-1} range. The surface morphology of the sample was studied with FESEM using a FESEM model (JSM-5910-JEOL JAPAN). The absorption phenomenon was recorded using aUV-2600 Shimadzu spectrophotometer at 580 nm (λ_{max} for CV) 490 nm (λ_{max} for CR) and 620 nm (λ_{max} for MG).

Adsorption Experiment. The effect of dye concentration, contact time, temperature, and pH on the adsorption of CV, CR, and MG was studied. Dye solutions ranging from 50 to 300 mL were brought in contact with 1 g of the activated adsorbent at different time intervals and different temperatures. Each of the solutions was filtered and analyzed spectrophotometrically using a UV-2600 Shimadzu spectrophotometer at 580 nm (λmax for CV), 490 nm (λmax for CR), and 620 nm (λmax for MG). Experiments were conducted at six different temperatures, namely, 283, 293, 303, 313, 323, and 333 K temperatures. The amount adsorbed in mg g^{-1} was determined through the following eq 9.

$$q_e = \frac{(C_i - C_e)}{W} \tag{9}$$

where q_e is the amount adsorbed in (mol·g^{-1}), C_i is the initial concentration in (mol·g^{-1}), C_e is the equilibrium concentration in (mol·g^{-1}), V is the volume of the solution, and W is the amount of adsorbent in grams.

AUTHOR INFORMATION

Corresponding Authors

Aiyeshah Alhodaib − *Department of Physics, College of Science, Qassim University, Buraydah 51452, Saudi Arabia*; Email: ahdieb@qu.edu.sa

Abid Zaman − *Department of Physics, Riphah International University, Islamabad 44000, Pakistan*; orcid.org/0000-0001-9527-479X; Email: zaman.abid87@gmail.com

Authors

Shah Hussain − *Department of Chemistry, Government Postgraduate College, Nowshera, Khyber-Pakhtunkhwa 24100, Pakistan*

Usman Ghani − *Department of Chemistry, Government Postgraduate College, Nowshera, Khyber-Pakhtunkhwa 24100, Pakistan*

Shahid Ali Khan − *Department of Chemistry, National University of Science and Technology, Islamabad 44000, Pakistan*

Vineet Tirth − *Mechanical Engineering Department, College of Engineering, King Khalid University, Abha 61421 Asir, Kingdom of Saudi Arabia; Research Center for Advanced Materials Science (RCAMS), King Khalid University, Abha 61413 Asir, Kingdom of Saudi Arabia*

Ali Algahtani − *Mechanical Engineering Department, College of Engineering, King Khalid University, Abha 61421 Asir, Kingdom of Saudi Arabia; Research Center for Advanced Materials Science (RCAMS), King Khalid University, Abha 61413 Asir, Kingdom of Saudi Arabia*

Asad Ali − *Department of Physics, Government Postgraduate College, Nowshera, Khyber Pakhtunkhwa 24100, Pakistan; Department of Physics, Riphah International University, Islamabad 44000, Pakistan*

Fozia Sultana − *Department of Chemistry, University of Science and Technology China, Hefei, Anhui 230026, P.R.China*

Muhammad Mushtaq − *Faculty of Materials and Manufacturing, Beijing University of Technology, Beijing 100124, China*

Complete contact information is available at: https://pubs.acs.org/10.1021/acsomega.2c00611

Author Contributions

This work was carried out in collaboration with all authors. S.H. and U.G. prepared samples and wrote the original draft of the article. A.Z., V.T., and A.A. did the final review writing, corrections, and editing. S.A.K. and A.A. helped in methodology and measurements. M.M. and F.S. prepared content analysis and graphical arrangements. A.A. helped in software, formal analysis, and providing funding acquisition. All authors have read and approved the final article.

Notes

The authors declare no competing financial interest.

ACKNOWLEDGMENTS

The researchers would like to thank the Deanship of Scientific Research, Qassim University, for funding the publication of this project. The authors gratefully acknowledge the Deanship of Scientific Research, King Khalid University (KKU), Abha-61421, Asir, Kingdom of Saudi Arabia, for funding this research work under the grant number RGP.2/225/43.

REFERENCES

(1) Ghani, U.; Hussain, S.; Noor-ul-Amin, M.; Imtiaz, M.; Khan, S. A. Laterite clay-based geopolymer as a potential adsorbent for the heavy metals removal from aqueous solutions. *J. Saudi Chem. Soc.* **2020**, *24*, 874−884.

(2) Hussain, S.; ul Amin, N.; Khan, S. A. Quartzite an efficient adsorbent for the removal of anionic and cationic dyes from aqueous solutions. *Arab. J. Chem.* **2020**, *13*, 4731−4740.

(3) Shah, S. A.; Ahmad, Z.; Khan, S. A.; Al-Ghamdi, Y. O.; Bakhsh, E. M.; Khan, N.; ur Rehman, M.; Jabli, M.; Khan, S. B. Biomass impregnated Zero-valent Ag and Cu supported-catalyst: Evaluation in the reduction of nitrophenol and discoloration of dyes in aqueous medium. *J. Organomet. Chem.* **2021**, *938*, 121756.

(4) Khan, S.; Anas, M.; Malik, A. Mutagenicity and genotoxicity evaluation of textile industry wastewater using bacterial and plant bioassays. *Toxicol. Rep.* **2019**, *6*, 193−201.
(5) Khan, S. A.; Bakhsh, E. M.; Asiri, A. M.; Khan, S. B. Chitosan coated NiAl layered double hydroxide microsphere templated zero-valent metal NPs for environmental remediation. *J. Clean. Prod.* **2021**, *285*, 124830.
(6) Khan, S. A.; Khan, S. B.; Asiri, A. M. Layered double hydroxide of Cd-Al/C for the mineralization and de-coloration of dyes in solar and visible light exposure. *Sci. Rep.* **2016**, *6*, 1−15.
(7) Puri, C.; Sumana, G. Highly effective adsorption of crystal violet dye from contaminated water using graphene oxide intercalated montmorillonite nanocomposite. *Appl. Clay Sci.* **2018**, *166*, 102−112.
(8) Fabryanty, R.; Valencia, C.; Soetaredjo, F. E.; Putro, J. N.; Santoso, S. P.; Kurniawan, A.; Ju, Y.-H.; Ismadji, S. Removal of crystal violet dye by adsorption using bentonite − alginate composite. *J. Environ. Chem. Eng.* **2017**, *5*, 5677−5687.
(9) Abidi, N.; Errais, E.; Duplay, J.; Berez, A.; Jrad, A.; Schäfer, G.; Ghazi, M.; Semhi, K.; Trabelsi-Ayadi, M. Treatment of dye-containing effluent by natural clay. *J. Clean. Prod.* **2015**, *86*, 432−440.
(10) Hussain, S.; Kamran, M.; Khan, S. A.; Shaheen, K.; Shah, Z.; Suo, H.; Khan, Q.; Shah, A. B.; Rehman, W. U.; Al-Ghamdi, Y. O.; Ghani, U. Adsorption, kinetics and thermodynamics studies of methyl orange dye sequestration through chitosan composites films. *Int. J. Biol. Macromol.* **2021**, *168*, 383−394.
(11) Ahmed, M. S.; Kamal, T.; Khan, S.; Anwar, Y.; Saeed, M.; Asiri, A. M.; Khan, S. B. Assessment of anti-bacterial Ni-Al/chitosan composite spheres for adsorption assisted photo-degradation of organic pollutants. *Curr. Nanosci.* **2016**, *12*, 569−575.
(12) Khan, S.; Khan, S.; Kamal, T.; Asiri, A.; Akhtar, K. Recent Development of Chitosan Nanocomposites for Environmental Applications. *Recent Pat. Nanotechnol.* **2016**, *10*, 181−188.
(13) Khan, S. A.; Khan, S. B.; Asiri, A. M. Toward the design of Zn−Al and Zn−Cr LDH wrapped in activated carbon for the solar assisted de-coloration of organic dyesr. *RSC Adv.* **2016**, *6*, 83196−83208.
(14) Xing, R.; Wang, W.; Jiao, T.; Ma, K.; Zhang, Q.; Hong, W.; Qiu, H.; Zhou, J.; Zhang, L.; Peng, Q. Bioinspired polydopamine sheathed nanofibers containing carboxylate graphene oxide nanosheet for high-efficient dyes scavenger. *ACS Sustainable Chem. Eng.* **2017**, *5*, 4948−4956.
(15) Gao, Y.; Guo, R.; Feng, Y.; Zhang, L.; Wang, C.; Song, J.; Jiao, T.; Zhou, J.; Peng, Q. Self-assembled hydrogels based on poly-cyclodextrin and poly-azobenzene compounds and applications for highly efficient removal of bisphenol A and methylene blue. *ACS Omega* **2018**, *3*, 11663−11672.
(16) Gopi, S.; Pius, A.; Thomas, S. Enhanced adsorption of crystal violet by synthesized and characterized chitin nano whiskers from shrimp shell. *J. Water Proc. Eng.* **2016**, *14*, 1−8.
(17) Kulkarni, M. R.; Revanth, T.; Acharya, A.; Bhat, P. Removal of Crystal Violet dye from aqueous solution using water hyacinth: Equilibrium, kinetics and thermodynamics study. *Resour.-Effic. Technol.* **2017**, *3*, 71−77.
(18) Quan, X.; Sun, Z.; Meng, H.; Han, Y.; Wu, J.; Xu, J.; Xu, Y.; Zhang, X. Polyethyleneimine (PEI) incorporated Cu-BTC composites: Extended applications in ultra-high efficient removal of congo red. *J. Solid State Chem.* **2019**, *270*, 231−241.
(19) Khan, S. A.; Khan, N.; Irum, U.; Farooq, A.; Asiri, A. M.; Bakhsh, E. M.; Khan, S. B. Cellulose acetate-Ce/Zr@ Cu0 catalyst for the degradation of organic pollutant. *Int. J. Biol. Macromol.* **2020**, *153*, 806−816.
(20) Gopinathan, R.; Kanhere, J.; Banerjee, J. Effect of malachite green toxicity on non target soil organisms. *Chemosphere* **2015**, *120*, 637−644.
(21) Murthy, T. P. K.; Gowrishankar, B. S.; Prabha, M. N. C.; Kruthi, M.; Krishna, R. H. Studies on batch adsorptive removal of malachite green from synthetic wastewater using acid treated coffee husk: Equilibrium, kinetics and thermodynamic studies. *Microchem. J.* **2019**, *146*, 192−201.
(22) Khan, S. A.; Khan, S. B.; Kamal, T.; Yasir, M.; Asiri, A. M. Antibacterial nanocomposites based on chitosan/Co-MCM as a selective and efficient adsorbent for organic dyes. *Int. J. Biol. Macromol.* **2016**, *91*, 744−751.
(23) Sheikh, Z.; Amin, M.; Khan, N.; Khan, M. N.; Sami, S. K.; Khan, S. B.; Hafeez, I.; Khan, S. A.; Bakhsh, E. M.; Cheng, C. K. Potential application of Allium Cepa seeds as a novel biosorbent for efficient biosorption of heavy metals ions from aqueous solution. *Chemosphere* **2021**, *279*, 130545.
(24) Kamranifar, M.; Khodadadi, M.; Samiei, V.; Dehdashti, B.; Noori Sepehr, M.; Rafati, L.; Nasseh, N. Comparison the removal of reactive red 195 dye using powder and ash of barberry stem as a low cost adsorbent from aqueous solutions: Isotherm and kinetic study. *J. Mol. Liq.* **2018**, *255*, 572−577.
(25) Babu, A. N.; Reddy, D. S.; Sharma, P.; Kumar, G. S.; Ravindhranath, K.; Mohan, G. V. K. Removal of Hazardous Indigo Carmine Dye from Waste Water Using Treated Red Mud. *Mater. Today Proc.* **2019**, *17*, 198−208.
(26) Jiang, Z.; Hu, D. Molecular mechanism of anionic dyes adsorption on cationized rice husk cellulose from agricultural wastes. *J. Mol. Liq.* **2019**, *276*, 105−114.
(27) Tahir, N.; Nawaz, B. H.; Munawar, I.; Saima, N. Biopolymers composites with peanut hull waste biomass and application for Crystal Violet adsorption. *Int. J. Biol. Macromol.* **2017**, *94*, 210−220.
(28) Tian, D.; Xu, Z.; Zhang, D.; Chen, W.; Cai, J.; Deng, H.; Sun, Z.; Zhou, Y. Micro−mesoporous carbon from cotton waste activated by FeCl3/ZnCl2: Preparation, optimization, characterization and adsorption of methylene blue and eriochrome black T. *J. Solid State Chem.* **2019**, *269*, 580−587.
(29) da Rosa, A. L. D.; Carissimi, E.; Dotto, G. L.; Sander, H.; Feris, L. A. Biosorption of rhodamine B dye from dyeing stones effluents using the green microalgae Chlorella pyrenoidosa. *J. Clean. Prod.* **2018**, *198*, 1302−1310.
(30) Bouras, H. D.; Yeddou, A. R.; Bouras, N.; Hellel, D.; Holtz, M. D.; Sabaou, N.; Chergui, A.; Nadjemi, B. Biosorption of Congo red dye by Aspergillus carbonarius M333 and Penicillium glabrum Pg1: Kinetics, equilibrium and thermodynamic studies. *J. Taiwan Inst. Chem. Eng.* **2017**, *80*, 915−923.
(31) Khan, S. A.; Arshad, T.; Faisal, M.; Shah, Z.; Shaheen, K.; Suo, H.; Asiri, A. M.; Akhtar, K.; Khan, S. B. Al−Sr metal oxides and Al−Cd layered double hydroxides for the removal of Acridine orange dye in visible light exposure. *J. Mater. Sci.: Mater. Electron.* **2019**, *30*, 15299−15312.
(32) Huang, B.; Lu, M.; Wang, D.; Song, Y.; Zhou, L. Versatile magnetic gel from peach gum polysaccharide for efficient adsorption of Pb2+ and Cd2+ ions and catalysis. *Carbohydr. Polym.* **2018**, *181*, 785−792.
(33) Gao, P.; Chen, D.; Chen, W.; Sun, J.; Wang, G.; Zhou, L. Facile synthesis of amine-crosslinked starch as an efficient biosorbent for adsorptive removal of anionic organic pollutants from water. *Int. J. Biol. Macromol.* **2021**, *191*, 1240−1248.
(34) Chaari, I.; Fakhfakh, E.; Medhioub, M.; Jamoussi, F. Comparative study on adsorption of cationic and anionic dyes by smectite rich natural clays. *J. Mol. Struct.* **2019**, *1179*, 672−677.
(35) Zhou, Y.; Luan, L.; Tang, B.; Niu, Y.; Qu, R.; Liu, Y.; Xu, W. Fabrication of Schiff base decorated PAMAM dendrimer/magnetic Fe3O4 for selective removal of aqueous Hg (II). *Chem. Eng. J.* **2020**, *398*, 125651.
(36) Azizian, S.; Eris, S.; Wilson, L. D. Re-evaluation of the century-old Langmuir isotherm for modeling adsorption phenomena in solution. *Chem. Phys.* **2018**, *513*, 99−104.
(37) Luan, L.; Tang, B.; Liu, Y.; Wang, A.; Zhang, B.; Xu, W.; Niu, Y. Selective capture of Hg (II) and Ag (I) from water by sulfur-functionalized polyamidoamine dendrimer/magnetic Fe3O4 hybrid materials. *Sep. Purif. Technol.* **2021**, *257*, 117902.
(38) Chen, Z.; Tang, B.; Niu, Y.; Chen, H.; Liu, Y.; Wang, A.; Bai, L. Synthesis of silica supported thiosemicarbazide for Cu (II) and Zn (II) adsorption from ethanol: A comparison with aqueous solution. *Fuel* **2021**, *286*, 119287.

https://doi.org/10.1021/acsomega.2c00611
ACS Omega 2022, 7, 12212−12221

(39) Liu, N.; Wang, H.; Weng, C.-H.; Hwang, C.-C. Adsorption characteristics of Direct Red 23 azo dye onto powdered tourmaline. *Arab. J. Chem.* **2018**, *11*, 1281−1291.

https://doi.org/10.1021/acsomega.2c00611
ACS Omega 2022, 7, 12212−12221